Vasopressin and angiotensin II differentially modulate human fear response dynamics to looming threats

Authors

Mengfan Han[1,2], Wenyi Dong[1,2], Kun Fu[1,2], Junjie Wang[1,2], Yuanhang Xu[1,2], Yueyuan Zheng[3], Keith M Kendrick[2], Ferraro Stefania[2], Ting Xu[4], Dezhong Yao[2], Benjamin Becker[1,5]*

Affiliations

[1] The Center of Psychosomatic Medicine, Sichuan Provincial Center for Mental Health, Sichuan Provincial People's Hospital, University of Electronic Science and Technology of China

[2] MOE Key Laboratory for Neuroinformation, School of Life Science and Technology, University of Electronic Science and Technology of China, Chengdu, China

[3] Division of Social Science, Hong Kong University of Science and Technology, Hong Kong, China

[4] Faculty of Psychology, Southwest University, Chongqing, China

[5] Department of Psychology, The University of Hong Kong, Hong Kong, China

* Corresponding author

E-mail: ben_becker@gmx.de (BB)

Abstract

While basal threat processing dynamics (e.g., visual looming) are well characterized in animals, the underlying mechanisms and their modulation by neuropeptide systems with different modulatory roles in threat processing (vasopressin, angiotensin II) remain poorly understood in humans. In a randomized, placebo-controlled eye-tracking study (*N*=111), we administered vasopressin (AVP) or an angiotensin II receptor blocker (via losartan, LT) during a time-to-collision threat paradigm. Behaviorally, AVP prolonged threat estimations, whereas LT reduced state anxiety. Pupillometry revealed distinguishable profiles: AVP induced sustained constriction during stimulus approach followed by post-stimulus threat-specific dilation, LT maintained sustained pupillary constriction throughout both approach and occlusion phases yet preserving threat-specificity, while placebo (PLC) showed no threat-specific modulation. A computational framework (combining functional principal component analysis [FPCA], clustering, and hidden Markov model [HMM]) underscored the distinct modulations: AVP promoted high loadings across components of vigilance, threat-specific anxiety, and perception-to-imagination transformation, indicating enhanced threat processing. LT suppressed transitions to high-arousal states and exhibited maximal sequence entropy, reflecting flexible response patterns—contrasting with placebo's lowest entropy dynamics. These results demonstrate that AVP and LT differentially regulate basal threat processing via separable neuropeptide pathways: AVP sustains hypervigilance while LT promotes anxiolysis and adaptive flexibility. Our findings suggest neuropeptide pathway-specific targets maladaptive threat processing in trauma- or anxiety-related disorders.

KeyWords

Threat, looming, vasopressin, angiotensin, pupillary dynamics, eye-tracking, phase-based pupillary analysis, functional linear mixed model (FLMM), functional principal component analysis (FPCA), hidden Markov model (HMM)

Abbreviations:

LT, losartan; PLC, placebo; AVP, arginine vasopressin; RAS, renin-angiotensin system; LC-NE, locus coeruleus-norepinephrine system; aTTC, actual time to collision; jTTC, judged time to collision; PSV, physical stimulus velocity; SBP, systolic blood pressure; DBP, diastolic blood pressure; Early/Late Imag, early/late imagination phase; FLMM, functional linear mixed model; FPCA, functional principal component analysis; PC, principal component; HMM, hidden Markov model

Introduction

The subjective experience of emotions varies across individuals and requires the coordinated involvement of distributed cortical and subcortical systems [1–3]. Some basic forms of 'primitive' affective mechanisms such as defensive reactions to rapidly approaching objects ('looming') appear to be innate, highly preserved across phylogenetic and ontogenetic evolution and tightly linked to specific (subcortical) circuits [4,5]. The visual system can for instance quickly detect impending collisions via estimating the accelerating expansion of objects on the retina (looming). Looming presents a fundamental, evolutionary and highly conserved threat detection mechanisms, which can be observed from fruit flies to humans [6,7]. This innate perceptual sensitivity to approaching stimuli that specifies the time-to-collision independent of size or distance enables

avoiding collisions and rapid defensive responses [8–10].

Although looming perception has been traditionally viewed as a basic visual computation, recent studies have demonstrated that looming is modulated by the semantic and affective content of the stimuli, such that threatening stimuli are typically underestimated in the time to collision by 20-30%, a time compression effect that may critically facilitate faster defensive reactions [10–12]. However, in natural environments, threatening objects such as predators often temporarily disappear from view, raising critical questions about how threat processing mechanisms operate without continuous visual input and how imagination maintains threat assessment during such periods. Understanding these mechanisms is crucial for developing ecologically valid models of threat processing and may help to determine how these processes can be targeted in mental disorders characterized by excessive threat processing.

The neuropeptide systems arginine vasopressin (AVP) and renin-angiotensin (RAS) have been associated with threat-related processing across species. AVP, synthesized in the hypothalamus, enhances threat processing by increasing the extended amygdala sensitivity to threat information and modulating prefrontal-amygdala circuits [13,14], with pronounced effects in males [15]. The RAS, in particular blockade of the RAS II AT1 receptors, has been associated with decreased fear by reducing amygdala reactivity to threat and enhancing prefrontal regulatory control [5,16–18]. While both systems influence threat processing through partially overlapping neural circuits and show complex synergistic effects in regulating physiological indices of threat responsivity including blood pressure and stress responses [19–21] their respective roles in looming threat processing remain to be explored.

Pupillary responses offer unique advantages as precise and non-invasive indicators of threat

processing dynamics [22–24]. Through tracking the activity of the locus coeruleus-norepinephrine (LC-NE) system pupil dilation provides high temporal resolution information about arousal related to cognitive and affective engagement [25,26], As such, pupil responses can reveal the continuous temporal dynamics of threat processing.

The LC-NE arousal system has shown a high sensitivity to both AVP [27] and RAS [28] modulation which render pupillary responses an ideal indicator for investigating the neurobiological basis of their modulatory role on threat processing.

Against this background we aimed at determining the role of two neuropeptide systems (AVP, RAS) in basal threat-related mechanisms, in particular to determine their effects on threat processing during looming via determining the effects of single dosages of both, AVP and a selective and competitive angiotensin receptor II antagonists (Losartan, LT) on behavioral and pupillary responses during the looming fear paradigm in combination with computational analytic approaches. This novel combination allows us to dissect the distinct contributions of these systems to threat processing and explore potential therapeutic implications. The hypothesized effects were tested in a pre-registered randomized placebo-controlled double-blind psychopharmacological eye tracking design during which participants were administered oral AVP, LT or placebo (PLC).

To provide an accurate test of the complex hypotheses we established a novel expansion of the threat looming paradigm and established a comprehensive analytic framework. This expansion integrates both visual and imagination components, comprising two phases: a one-second 'visual stimulus amplification' phase providing initial approach velocity information, followed by an 'imagined stimulus approach' phase where the visual threat stimulus disappears after the approach information has been acquired. This design builds on substantial evidence that threat-related

neural systems remain active even without direct visual input [29,30], and amygdala-centered defensive circuits continue processing threats when visual stimuli are subliminal or masked [31,32], indicating robust threat maintenance mechanisms during temporary visual occlusion.

To characterize the complex dynamics of threat processing, we developed an integrated analytical framework combining pupillary features, behavioral responses, and temporal measurements. This multivariate approach identifies distinct threat response patterns and their pharmacological modulation through dimensional reduction and clustering techniques. By simultaneously analyzing multiple pupillary characteristics and behavioral measures, we reveal how different pharmacological treatments shape overall threat processing strategies. This systematic approach advances beyond traditional univariate analyses to capture the temporal evolution and multidimensional nature of threat responses under different pharmacological conditions.

Our specific aims in this study were to: (1) characterize threat processing dynamics during looming through pupillary responses, (2) examine the maintenance of threat perception during visual occlusion, (3) investigate pharmacological modulation of the identified threat processes, and (4) identify distinct response patterns through Functional Principal Component Analysis–clustering–Hidden Markov Model (FPCA–clustering–HMM) analysis. The findings may reveal innovative targets for testing novel interventions for disorders characterized by elevated threat reactivity and have important implications for how neuropeptides shape defensive behaviors.

Methods

1. Participants and Study Design

1.1 Participants

Following evaluated recruitment criteria, 111 healthy volunteers (n = 37 per treatment group) were included in the final analysis (details see CONSORT flowchart in S1 Fig). Sample size was a priori determined using G*Power for a 3 (Treatment) × 2 (Sex) × 2 (IsThreaten) × 2 (Initial width) × 5 (actual Time-To-Collision, aTTC) mixed-design ANOVA, resulting in a required sample size of 90 (f = 0.25, α = 0.05, power = 0.80).

Eligible participants had normal or corrected-to-normal vision, no history of psychiatric/neurological disorders, no current medication use, and no substance use including nicotine. All participants underwent electrocardiogram (ECG) examination within one week before testing and were required to abstain from caffeine and alcohol for 24 hours prior to participation. Female participants were tested for pregnancy on the day of the experiment.

The study was approved by the local ethics committee of University of Electronic Science and Technology of China (UESTC), conducted according to the Declaration of Helsinki, and pre-registered (ClinicalTrials.gov ID: NCT06329063, NCT06329076). All participants provided written informed consent and received monetary compensation (140 RMB).

1.2 Study Design

In a randomized, double-blind, placebo-controlled pharmacological behavioral and eye-tracking design, participants were randomly assigned using computer-generated sequences to receive either AVP, LT, or PLC (mean age ± SD: 22.33 ± 2.22 years; no significant age differences between groups, $F(2,108) = 2.13$, $p = .12$).

2. Experimental Procedures

2.1 Baseline Assessments

Prior to drug administration, participants completed validated Chinese versions of standardized questionnaires assessing affective states and fear-related traits, including the Positive and Negative Affect Schedule (PANAS) [33]; State-Trait Anxiety Inventory (STAI) [34]; Liebowitz Social Anxiety Scale (LSAS) [35]; and Animal Fear Questionnaire (AFQ) [36]. Female participants' menstrual cycle phases were documented following established procedures [37,38]. To control for unspecific effects due to an impact of treatment on cardiovascular parameters, blood pressure and heart rate were monitored at three time points: pre-drug administration (baseline), peak drug effect (45 min post-administration for AVP group, 90 min post-administration for LT group), and post-experiment completion (similar in [18,39], Fig. 1A).

2.2 Drug Administration

Treatment doses were selected based on previous research demonstrating efficacy in modulating social-emotional processing including fear-related processes: 20 IU AVP [39] and 50 mg LT [16–18].

We employed a novel spray-based oral delivery method for AVP administration [40], offering more precise assessment of peripheral effects by preventing direct olfactory system entry [41]. AVP (Bio-Techne China Co., Ltd) was stored at -20°C and prepared as a sterile spray (0.22 μm Millipore filtered) containing AVP dissolved in saline and glycerol. Following our validated protocol, participants received six alternating 0.1 ml puffs (three to the superior and three to the

inferior surface of the tongue, with 30-second retention periods between puffs). Placebo sprays were identical in composition but excluded AVP. The LT group received visually matched capsules containing either 50 mg Losartan or no active ingredient.

To ensure effects of both treatments during peak plasma windows (based on established pharmacokinetic profiles showing peak effects at 45 min for AVP and 90 min for LT) and to ensure double-blinding during experimental tasks, we implemented a two-stage administration protocol:

- Group 1: 50 mg LT capsule (90 min pre-task) + PLC spray (45 min pre-task)
- Group 2: PLC capsule (90 min pre-task) + PLC spray (45 min pre-task)
- Group 3: PLC capsule (90 min pre-task) + 20 IU AVP spray (45 min pre-task)

All treatments were administered by research staff blind to treatment conditions. Post-experiment treatment guesses by participants were not better than chance level, confirming successful blinding (χ^2= 0.83 p = .36).

2.3 Experimental Task

The study employed a validated threat looming paradigm [10] utilizing color photographs of threatening (categories: snakes, spiders) and non-threatening (butterflies, rabbits) animals. Images (n = 40 per category) were normalized using Adobe Photoshop to 400×250 pixels with uniform grey backgrounds. Stimuli were presented using Psychotoolbox-3 in MATLAB (R2018b).

Each trial (Fig. 1B) included three presentation phases: (1) a central fixation cross (300ms), (2) a looming stimulus expanding at a constant velocity for 1000ms, and (3) an imagination phase after stimulus disappearance. The initial stimulus width was 256 or 384 pixels (20% or 30% of

screen width), with expansion velocities determined by five predefined actual Time-to-Collision (aTTC) values (3.0, 3.5, 4.0, 4.5, and 5.0s). Participants imagined the stimulus continuing its approach at the same velocity after disappearance and pressed the spacebar when they judged it would collide with them, providing a judged Time-to-Collision (jTTC). A beep indicated response registration, followed by a jittered inter-trial interval of 1000-3000ms.

The experiment comprised 160 trials in two blocks, with factorial combination of aTTC (5 levels), stimulus category (4 levels), and initial size (2 levels). Trial order was randomized within blocks. Prior to the main task, participants completed 20 practice trials using animal silhouettes to familiarize themselves with all experimental conditions.

The task duration was approximately 30 minutes, with self-paced breaks between blocks. For each trial, jTTC was measured, with continuous pupillary recording throughout.

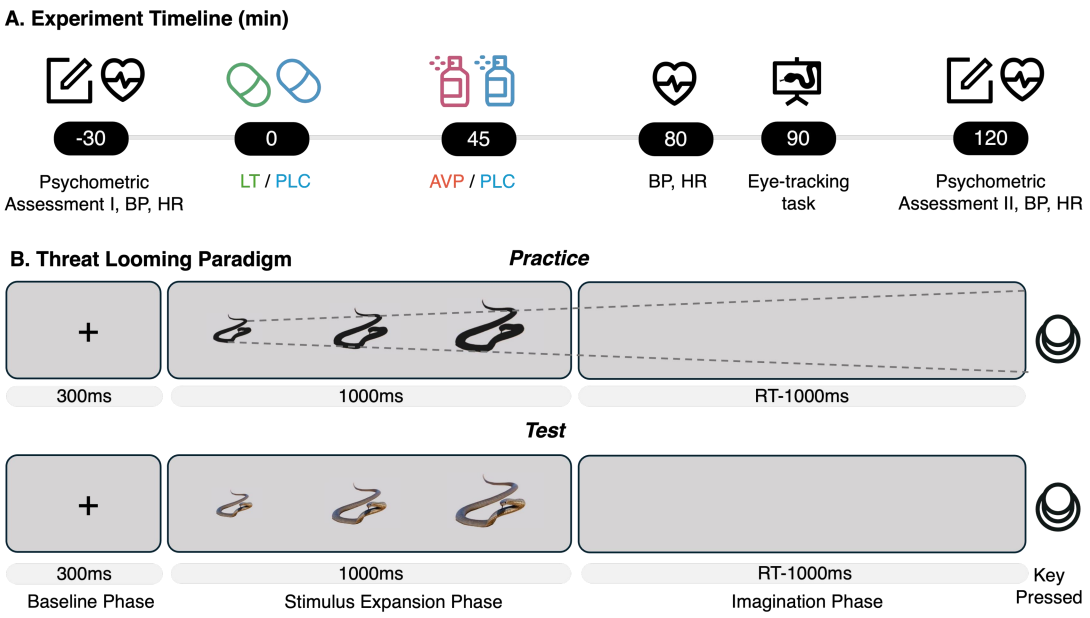

Fig 1. Experimental timeline and task structure. (A) Sequence of drug administration and behavioral testing. **(B)** Single trial structure of the threat looming task.

3. Data Acquisition and Preprocessing

3.1 Behavioral Data Preprocessing

Trial-level jTTC data were preprocessed using a two-stage protocol: First, trials with technical artifacts or incomplete responses were excluded. Second, trials exceeding ±5 SD from each participant's mean jTTC were identified as potential outliers. This conservative criterion preserved potential treatment-induced variations while flagging extreme deviations, following methodological recommendations for pharmacological studies [42,43].

3.2 Pupillary Data Preprocessing

Right eye pupil size and movements were recorded at 2000 Hz using an EyeLink 1000 Plus system (SR Research, Ottawa, Canada) with a display resolution of 1280 × 1024 pixels. Participants were positioned 57 cm from the monitor using a chin rest to maintain stable head position. A 9-point calibration procedure at the beginning of each experimental block and a drift check before each trial were applied to ensure optimal tracking accuracy.

Pupil size was recorded as pixel area and converted to diameter (d) using:

$$d = \alpha L \varphi$$

where α represents an empirically derived scaling factor, L denotes the pupil-to-camera distance, and φ is the visual angle (computed as the square root of the measured pupil area [44]).

Pupillary data underwent systematic preprocessing to remove: (1) periods of signal loss, (2) blink-related artifacts (±20ms surrounding blinks, defined as >0.3mm changes between consecutive samples or signal loss), (3) physiologically implausible values (diameter = 0 or >9.8mm, rate of change >0.64mm/s), and (4) statistical outliers exceeding ±5 SD from the trial

mean. These criteria were implemented following established pupillometry guidelines [25]. The preprocessed data were subsequently averaged into 10ms bins to attenuate high-frequency noise while preserving physiologically meaningful signals [45].

3.3 Stimulus Dynamics

To optimize analyses, we derived a composite measure of stimulus dynamics by computing Physical Stimulus Velocity $\mathrm{PSV} = (\mathrm{ScreenWidth} - \mathrm{InitialWidth}/\mathrm{aTTC})$, consolidating looming motion parameters into a single ecologically relevant metric. Approach velocities (179.2-341.3 pixels/s) were divided into five equal intervals: very slow (V1: 179.2-211.6), slow (V2: 211.6-244.0), medium (V3: 244.0-276.4), fast (V4: 276.4-308.8), and very fast (V5: 308.8-341.3 pixels/s), with right-closed intervals. These velocity categories (V1-V5) were used as levels in subsequent analyses.

4 Analysis Framework

4.1 Behavioral Analysis

A mixed-design ANOVA was conducted on jTTC with Treatment (LT, PLC, AVP) and Sex(female, male) as between-subject factors, and IsThreaten (threatening, non-threatening) and PSV (V1-V5) as within-subject factors. Pre-registered contrasts compared AVP vs. PLC and LT vs. PLC.

4.2 Baseline Analysis

We first conducted a two-way ANOVA to examine Treatment and Sex effects on baseline

pupil diameter (0-300ms), aiming to distinguish general from domain-specific treatment effects. To isolate task-specific pupillary responses from general drug effects, all subsequent analyses used baseline-corrected data. While this correction masks potential treatment effects on absolute pupil size, it allows for direct comparison of task-induced pupillary dynamics by normalizing baseline differences across conditions.

4.3 Event-Locked Phase Analysis

Based on the baseline-corrected data, we analyzed pupillary responses in three functionally distinct phases: Stimulus Presentation (300-1300ms; encoding of the approaching stimulus), Early Imagination (first 500ms following stimulus disappearance), and Late Imagination (last 500ms before estimated collision).

The selection of these temporal windows reflects key task phases and physiological response characteristics. The stimulus presentation phase captures pupillary responses during active visual processing of the approaching stimulus, covering the entire visual motion sequence [30]. The early imagination phase examines immediate pupillary dynamics following transition to mental representation [46], while the late imagination phase focuses on decision-related responses [47]. This novel temporal segmentation allows examination of threat perception dynamics during both visual processing and imagination phases.

These phases were analyzed using repeated measures ANOVA with Treatment and Sex as between-subject factors, and Phase, IsThreaten, and PSV as within-subject factors. Trials shorter than 2300ms (2% of total) were excluded to ensure sufficient duration for reliable phase analysis.

4.4 Time-Normalized Dynamic Analysis

Variable trial durations, primarily resulting from individual differences in estimated time-to-collision, pose challenges for examining dynamic pupillary response patterns across trials. Without standardization, direct comparison of temporal dynamics becomes problematic. Therefore, we implemented temporal normalization procedures to enable systematic cross-trial comparisons.

For the preprocessed and downsampled data (100 Hz), we applied a piecewise linear time warping approach to normalize trial durations. Each trial was divided into two functionally distinct epochs: stimulus presentation (300-1300ms) and imagination period (1300ms to response). These epochs were separately mapped onto fixed segments of a normalized time scale [0,1], with stimulus presentation occupying [0,0.5] and imagination period occupying [0.5,1.0].

For each normalized epoch, we employed equidistant temporal sampling to extract 100 points, resulting in 200 uniformly distributed sampling points across the complete trial. This approach preserves the relative temporal structure within each functional epoch while standardizing overall trial duration. The normalized pupillary time series were fitted using cubic B-spline functions (order 3, 4 basis components), with parameters determined through generalized cross-validation which helps reduce noise while preserving the underlying temporal dynamics.

Trials were excluded based on predefined quality criteria including missing responses, insufficient valid data points (<10 overall or <3 per phase), short duration (<2300ms), and poor signal integrity (verified through temporal continuity and autocorrelation analysis). This resulted in 14,266 valid trials (90.35%) for analysis.

To examine task-induced dynamic changes in pupillary responses, we fitted functional linear mixed models (FLMM) with fixed effects of Treatment, Sex, IsThreaten, PSV, and their

interactions, including by-subject random intercepts and random slopes for Normalized_Time, IsThreaten, and PSV. The model is specified as:

$$\text{Baseline - corrected Pupil Diameter} \sim \text{Treatment} \times \text{Sex} \times \text{IsThreaten} \times \text{PSV} \times \text{Normalized_Time} + (\text{Normalized_Time} + \text{IsThreaten} + \text{PSV} \mid \text{Subject})$$

This approach integrates event-locked phase analysis (comparing theoretically important time windows) with FLMM-based dynamic modeling capturing temporal continuity in attention and emotional processing during threat perception, providing a comprehensive characterization of pupillary response patterns during threat perception.

4.5 Integrated Pattern Analysis

We developed an integrated analytical framework combining Functional Principal Component Analysis (FPCA), clustering and Hidden Markov Models (HMM) to characterize comprehensive behavioral-physiological response patterns and their temporal evolution. This approach captures both behavioral-pupillary features and state transition dynamics, enabling systematic evaluation of pharmacological interventions on threat processing.

Using FPCA, which better accounts for temporal continuity compared to traditional PCA [48], we extracted principal temporal response patterns (eigenfunctions) from time-normalized pupillary data within each trial. This dimensional reduction approach yielded multiple functional components per trial that collectively characterized the complete temporal dynamics of pupillary responses. We retained principal components that explained over 85% of total variance (individual components >5%) and examined their associations with experimental conditions, individual characteristics, and pupillary features during and after stimulus presentation.

To classify trials into distinct response patterns based on their behavioral-physiological

characteristics, we integrated the FPCA components with behavioral features (jTTC) using a hierarchical k-means clustering framework. Given their different measurement scales, we first clustered on log-transformed jTTC, then on FPCA components within each temporal group. Optimal cluster numbers were determined using Calinski-Harabasz index and silhouette coefficients, with clustering stability verified through bootstrap resampling (n=1000, stability index>0.85) and cross-validation (accuracy>0.80).

We then analyzed pattern transitions using first-order Hidden Markov Models (HMM), treating each trial as a discrete time point. The analysis was conducted through three levels:

(1) At the distribution level, we obtained steady-state distributions and used chi-square tests with standardized residual analysis to examine pattern distribution differences across experimental conditions.

(2) At the transition level, we analyzed state transition probability matrices, using bootstrap methods (n=1000) to identify significant transitions across treatments and threat states.

(3) At the sequence level, we analyzed three-state continuous sequences and calculated state sequence entropy to quantify the complexity of pattern transitions across conditions.

4.6 Analytic Software and Correction

Behavioral analyses and event-locked phase analyses were conducted using SPSS 26. Time-normalized dynamic analyses and integrated pattern analyses were implemented in Python v3.12 using scientific computing libraries (pandas, numpy, scipy, statsmodels, scikit-learn) with custom implementations for functional data analysis. For all analyses, effects were considered significant at $p < .05$ with Greenhouse-Geisser correction for sphericity violations. Multiple

comparisons were controlled for false discovery rate using the Benjamini-Hochberg method (α = 0.05).

Results

1 Subjective Anxiety and Potential Confounders

The three groups (LT, PLC, and AVP; n = 37 each) did not differ in age, mood, animal fear, or personality traits (all ps > .13, S1 Table). A 2 (Treatment: LT vs. PLC) × 2 (Sex: male vs. female) × 2 (Time: pre vs. post) mixed ANOVA with State Anxiety as the dependent variable revealed a significant Treatment × Time interaction (F = 4.11, p = .047, η_p^2 = 0.055). Between-group comparison showed lower post-task state anxiety level in the LT group compared to PLC (p = .012, d = 0.51) which was mirrored in within-group analyses indicating significant anxiety reduction in the LT group (pre: 37.51 ± 1.10, post: 33.39 ± 1.36, p = .005, dz = 0.58) but not in the PLC group (pre: 38.44 ± 1.10, post: 38.36 ± 1.35, p = .95, dz = 0.02). This may suggest an anxiolytic effect of LT (Fig 2A). No such pattern emerged for AVP (Treatment × Time, p = .78). Critically, the anxiety-reducing effect of LT did not differ by sex (ps > .41).

Cardiovascular parameters (systolic blood pressure, diastolic blood pressure, and heart rate) were monitored at three time points: baseline, drug peak effect (80 minutes post-LT; 35 minutes post-AVP), and post-task. Mixed ANOVAs revealed only a main effect of sex, with males showing higher resting blood pressure than females (SBP: 118.17 ± 0.74 vs. 110.34 ± 0.74 mmHg, p < .001; DBP: 73.66 ± 0.85 vs. 71.18 ± 0.85 mmHg, p = .041) (Fig 2B). No significant treatment effects or interactions were found at any time point (all ps > .10).

2 Time-to-collision Analysis

Analysis of judged time-to-collision (jTTC) showed that threatening stimuli induced shorter time estimations compared to non-threatening ones ($F = 30.04$, $p < .001$, $\eta_p^2 = 0.22$), with females showing overall shorter estimations ($F = 5.46$, $p = .021$, $\eta_p^2 = 0.049$). Higher approaching velocities predictably led to shorter estimations ($F = 50.6$, $p < .001$, $\eta_p^2 = 0.67$).

These main effects were accompanied by two significant interactions. The PSV × IsThreaten interaction ($F = 9.23$, $p < .001$, $\eta_p^2 = 0.266$) revealed that threat-induced temporal compression was present across velocities V1-V4 but disappeared at V5 (fastest velocity) (Fig 2C). This finding reflects successful threat induction via looming and an affective (threat) modulation of the effect. Similarly, the Sex × PSV interaction ($F = 4.71$, $p = .002$, $\eta_p^2 = 0.156$) showed that females exhibited shorter time estimations than males across velocities V1-V4, while this sex difference disappearing at V5.

While no overall treatment effect (LT, PLC, AVP) was found ($F = 2.19$, $p = .17$), planned comparisons between AVP and PLC revealed a main effect of treatment, with AVP significantly prolonging time estimations ($F = 4.19$, $p = .044$, $\eta_p^2 = 0.056$) (Fig 2D). No significant difference was observed between LT and PLC.

3 Baseline Analysis

Analysis of pre-stimulus baseline pupil diameter (0-300ms) revealed a significant main effect of treatment ($F = 4.31$, $p = .016$, $\eta_p^2 = 0.076$). The AVP group exhibited significantly larger baseline diameters (2.52 ± 0.41mm) than the PLC group (2.28 ± 0.23mm, $p = .011$), while the LT group showed intermediate values (2.42 ± 0.34mm; AVP vs LT: $p = .203$; LT vs PLC: $p = .104$).

No sex-related effects were significant (*p*s > .2).

The treatment-dependent pattern (AVP > LT > PLC) persisted across trials in uncorrected pupil data (F = 3.98, p = .023; Fig 2E). Baseline correction was therefore applied and eliminated these general treatment-related differences (*p*s > .12), allowing us to examine task-specific changes in pupillary responses (detailed in Sections 4-6).

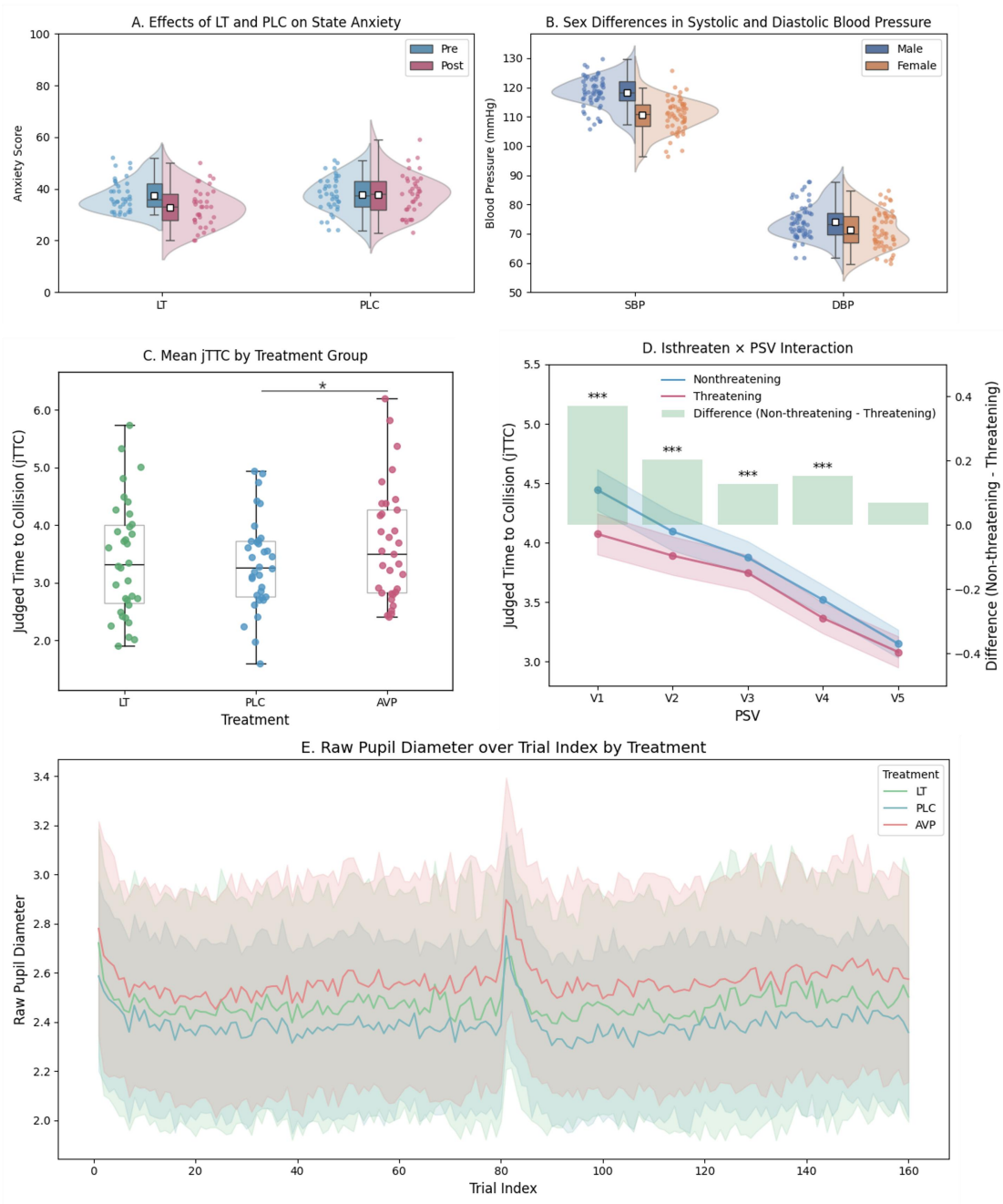

Fig 2. Physiological Measures and Behavioral Results. (A) State anxiety scores before and after the experiment in LT and PLC groups. **(B)** Sex differences in blood pressure (SBP, DBP). White squares within box plots represent mean values for A and B. **(C)** Mean judged time-to-collision (jTTC) for different treatment groups (LT, PLC, and AVP). Individual data points are overlaid. **(D)** Time-to-collision judgments under threatening (red) and non-threatening (blue) conditions across velocities (V1-V5). Green bars show their differences (right y-axis). **(E)** Uncorrected raw pupil diameter by treatment group (AVP: red, LT: green, PLC: blue) across trials, with 95% confidence intervals. Break occurred at trial 80. *p<.05, ***p < .001.

4 Event-Locked Phase Analysis

Phase-locked analysis of baseline-corrected pupil responses revealed significant main effects of Phase (F = 41.97, p < .001, η_p^2 = 0.446) and PSV (F = 19.92, p < .001, η_p^2 = 0.429). Pupil diameter increased from stimulus presentation (-0.001 ± 0.003mm) to early imagination (0.039±0.006mm, p < .001) and stabilized during late imagination (0.044±0.005mm, Early vs Late Imag: p = .22). Extreme velocities (V1/V5) elicited larger response than moderate velocities (V2-V4, ps < .01).

Several Phase-related interactions emerged, with experimental conditions showing no differences during stimulus presentation but diverging during imagination phases.

Phase × IsThreaten interaction (F = 16.20, p < .001, η_p^2 = 0.238) revealed that during late imagination, threat-induced pupil dilation was significantly larger than for non-threatening stimuli (p = .004). Across phases, threatening stimuli induced progressive dilation (Stim < Early Imag < Late Imag, ps < .05), while non-threatening stimuli caused initial dilation followed by plateau

(Stim < Early Imag ≈ Late Imag, *p*s < .01) (Fig 3A).

Phase × Treatment interaction (F = 2.93, p = .022, η_p^2 = 0.053) indicated that during early imagination, PLC group showed higher responses (0.062 ± 0.011mm) than both LT (0.028 ± 0.011mm, p = .033) and AVP groups (0.026±0.011mm, p = .023), while no group differences emerged during stimulus presentation or late imagination (*p*s > .22). Across phases, AVP group showed progressive dilation (Stim < Early Imag < Late Imag, *ps* < .05), while LT and PLC groups showed initial dilation followed by plateau (Stim < Early Imag ≈ Late Imag, *p*s < .01) (Fig 3B).

IsThreaten × PSV interaction (F = 4.37, p < .01, η_p^2 = 0.143) revealed velocity-dependent threat processing: under non-threatening conditions, only V5 enhanced responses compared to V1-V4 (*p*s < .05), while threat amplified responses to both extreme velocities (V1/V5 > V2-V4, *p*s < .01). Furthermore, threatening compared to non-threatening stimuli enhanced responses at V1 and V4 (ps < .05) but attenuated responses at V2 (p = .028) (Fig 3C).

IsThreaten × Sex interaction (F = 18.513, p < .001, η_p^2 = 0.143) showed that males exhibited larger baseline responses than females for non-threatening stimuli (p = .003), but no sex difference under threatening condition (p = .84). Females showed stronger responses to threatening compared to nonthreatening stimuli (p < .001), while males' responses remained consistent across threat conditions (p = .10) (Fig 3D).

5 Time-Normalized Dynamic Analysis

Functional linear mixed models (FLMM) with baseline-corrected pupil diameter as the dependent variable were conducted, using PLC group, non-threatening condition, moderate stimulus velocity (V3), and male participants as reference levels.

Analyses revealed overall pupil dilation with normalized time (β = 0.010, p = .030) and threat-induced constriction (β = -0.016, p < .001). PSV demonstrated a V-shaped velocity-dependent pattern, with maximal dilation at extreme velocities (V1/V5: β = +0.016/+0.018), moderate dilation at V2 (β = +0.005), and no change at V4 relative to V3 (ps < .001, except V4: p = .63).

Extending phase-locked findings, FLMM revealed more nuanced interaction patterns:

Treatment effects on threat processing evolved across time. All groups showed initial threat-induced constriction during approach and offset (βs = -0.001-0.012, ps < .001). Before anticipated collision, threat versus non-threat comparison showed no difference in PLC (p = .76), but significant dilation under threatening condition in both LT and AVP groups (β = 0.009/0.016, ps < .001). Between-treatment comparisons revealed sustained constriction in LT versus PLC, while AVP showed a distinct pattern: initial constriction followed by enhanced dilation after post-stimulus, particularly under threat (β = 0.008, p < .001). In conclusion, LT enhanced pupillary responses to imaginary threats while maintaining smaller baseline diameter, whereas AVP induced a distinctive pattern shift from constriction to dilation under threat conditions (Fig 3E1: AVP vs PLC; Fig 3E2: LT vs PLC).

The Treatment × IsThreaten × PSV interaction revealed distinct pupillary response patterns across conditions (βs = 0.001-0.002, ps < .01). Between-group comparisons consistently showed stronger responses in PLC compared to both AVP and LT groups (βs = 0.017-0.041, ps < .05). The AVP group reached its lowest point at V4 and consistently showed larger responses to threatening versus non-threatening stimuli across all velocities (V1-V5: βs = 0.0028-0.0099, ps < .001). The LT group's response also reached its lowest point at V4, but threat > non-threat differences

emerged only at faster velocities (V3-V5: β = 0.005-0.0097, *p*s<.001), while the PLC group reached its lowest response at V3 and showed no consistent velocity-specific threat sensitivity. These findings indicate that PLC group showed the largest overall pupillary responses, AVP showing reduced pupillary responses but preserved threat sensitivity, and LT selectively increased threat responses at faster velocities (Fig 3F).

Sex × IsThreaten × Normalized Time interaction (β = 0.025, p < .001) revealed distinct temporal patterns in pupillary responses between sexes. During the stimulus approach, males exhibited significantly larger pupil dilation than females across both threatening and non-threatening conditions (t = 0.25, β = 0.0051; t = 0.5, β = 0.0208, *p*s < .001). Both males and females showed greater pupillary responses to non-threatening versus threatening stimuli (males: β = 0.0047, p < .001; females: β = 0.0008, p < .05). At anticipated collision (t = 1.0), male>female persisted in the non-threatening condition (β = 0.0221, p < .001) but disappeared in the threatening condition (β = -0.0004, p = .61). Within-group analyses revealed that males showed no threat-related differences (p > .05), while females demonstrated a significant reversal pattern, with threatening stimuli eliciting substantially greater pupillary dilation compared to non-threatening stimuli (β = -0.0193, p < .001) (Fig 3G). Further examination of treatment-specific sex differences revealed distinct modulatory effects across groups. In the PLC group, females showed greater dilation than males across conditions (βs = 0.018-0.021, *p*s < .001). In contrast, under LT females showed s stronger constriction relative to males (βs = -0.017-0.027, *p*s < .01). The AVP group showed condition-dependent effects: females exhibited stronger constriction in non-threat (β = 0.017, p < .01), but no sex difference emerged under threat (p = .58).

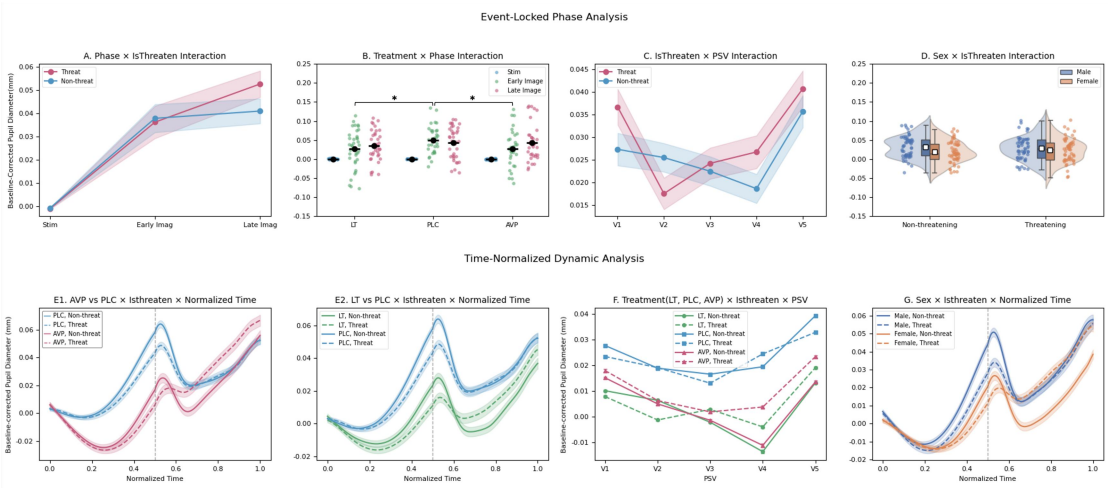

Fig 3. Pupillary Measurement Results: Phase-Locked and Normalized Time Analyses. Panels A-D show phase-locked analysis results while E-G present normalized time analysis. Shaded areas/error bars indicate ±1 SEM; vertical gray lines (t=0.5) mark stimulus offset. **(A)** The Phase × IsThreaten interaction revealed significant pupil dilation to threatening compared to non-threatening stimuli during late imagination (p=.004). Threatening stimuli induced progressive dilation (Stim < Early Imag < Late Imag; ps < .05), while non-threatening stimuli showed initial dilation followed by plateau (Stim < Early/Late Imag; ps < .01). **(B)** The Treatment × Phase interaction demonstrated significantly larger pupils in the PLC group compared to AVP and LT groups during early imagination (ps < .05), with no significant treatment differences during stimulus presentation or late imagination. Across phases, the AVP group showed continuous dilation, while PLC and LT groups exhibited initial dilation followed by plateau. **(C)** The IsThreaten × PSV interaction showed selective dilation at highest velocity under non-threat conditions (V5 > V1-V4, p < .05), whereas threat enhanced responses at both velocity extremes (V1/V5 > V2-V4, ps < .05). Threat enhanced responses at V1 and V4 (ps < .05) but reduced responses at V2 (p = .028), creating a V-shaped distribution with minimum pupil size at V2 for threatening and V4 for non-threatening stimuli. **(D)** The Sex × IsThreaten interaction revealed

larger pupillary responses in males under non-threatening conditions (p = .003), with sex differences diminishing during threat exposure. **(E1)** AVP vs PLC × IsThreaten × Normalized time: During stimulus approach, both AVP and PLC groups showed stronger pupillary responses to non-threatening than threatening stimuli. However, AVP group exhibited response reversal before anticipated collision, with significantly stronger responses to threatening stimuli. Between-group comparisons showed larger pupils in the PLC group during approach phase, but significantly larger pupils in the AVP group before anticipated threatening collision. **(E2)** LT vs PLC × IsThreaten × Normalized time: LT group consistently showed smaller pupils than PLC group across time. During approach, both groups exhibited pupil constriction to threatening versus non-threatening stimuli, but before anticipated collision, LT group showed greater dilation to threatening than non-threatening stimuli, while threat-related pupillary differences disappeared in the PLC group. **(F)** Treatment (LT, PLC, AVP) × IsThreaten × PSV interaction revealed V-shaped response patterns across velocity points in all treatment groups, with notable differences: PLC group showed overall stronger responses reaching minimum at moderate velocity (V3); AVP group reached minimum at V4 and enhanced threat responses across all velocities; LT group also reached minimum at V4 but selectively enhanced responses to faster threatening stimuli. Between-group comparisons consistently showed PLC > AVP and PLC > LT, confirming AVP comprehensively enhanced threat sensitivity while LT selectively enhanced pupillary responses to rapidly approaching threatening stimuli. **(G)** Sex × IsThreaten × Normalized time: During stimulus approach, males showed greater dilation than females in both conditions; both sexes initially responded more strongly to non-threatening stimuli; at anticipated collision point, males maintained larger responses than females under non-threatening conditions, but sex differences

disappeared under threat; notably, males showed no significant differentiation between threatening and non-threatening conditions, while females exhibited a reversal pattern with significantly greater threat-induced pupil dilation at collision point, demonstrating female-specific threat sensitivity.

6 Integrated Pattern Analysis

6.1 Functional Principal Component Decomposition

FPCA analysis of baseline-corrected pupil diameter revealed that the first three principal components accounted for 87.51% of the total variance (PC1: 62.7%, PC2: 17.6%, PC3: 7.3%). These components captured distinct patterns of pupillary dynamics as illustrated in Fig 4.

PC1 revealed a monophasic pattern with consistently positive weights that increased from 0.20 to 1.20 before plateauing, representing sustained pupillary dilation throughout the observation period.

PC2 demonstrated a biphasic pattern, with weights initially negative (-0.40 to -1.20) during the first half of the trial, followed by a rapid increase to positive values (peaking at 1.50) in the final fifth of the trial, indicating a transition from initial constriction to later dilation.

PC3 exhibited a triphasic pattern with weights that were initially positive (peaking at 1.80 at 0.1 normalized time), then sharply decreased to negative values (minimum -1.30 at 0.55 normalized time), before gradually returning to positive values (0.80), suggesting complex regulatory dynamics.

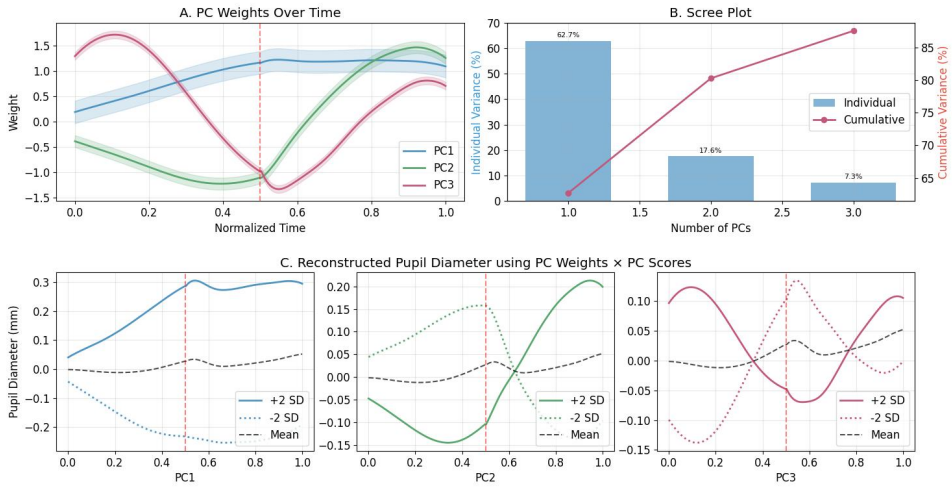

Fig 4. Principal component analysis of pupillary features. (A) Temporal weight functions showing the contribution of PC1-3 over normalized time. The solid lines represent the mean weights, with shaded areas indicating the 95% confidence intervals. The vertical dashed red line marks the stimulus onset. **(B)** Scree plot displaying both individual (blue bars) and cumulative (red line) explained variance for the first three PCs. PC1, PC2, and PC3 account for 62.7%, 17.6%, and 7.3% of the total variance respectively, with a cumulative explained variance of 87.6%. **(C)** Reconstructed pupil diameter changes based on PC weights × PC scores for PC1-3. For each PC, the solid line represents pupil diameter changes at +2 SD of PC scores, the dotted line at -2 SD, and the dashed line shows the mean response. Changes in pupil diameter are shown in millimeters (mm).

Effects of Experimental Conditions on Principal Components

Mixed ANOVAs on the principal components (PC1-3) revealed distinct effects of experimental conditions (Fig. 5).

All components showed significant PSV main effects (PC1: $F = 105$, $p < .001$, $\eta_p^2 = .40$; PC2:

F = 105, p < .001, η_p^2 =.31; PC3: F = 7.32, p = .005, η_p^2 =0.63), each with distinct patterns: extreme speeds (V1, V5) elicited higher PC1 loadings but lower PC3 loadings than medium speeds (V2-V4), while PC2 showed progressively increased loadings with speed (Fig. 5C).

For PC1 (sustained dilation pattern), we found a significant Treatment × Sex × Isthreaten interaction (F = 3.37, p = .023, η_p^2 =0.69). Females showed treatment-dependent responses to threat: under non-threatening conditions, the PLC group exhibited higher PC1 loadings than drug groups (ps < .01), while under threatening conditions, both PLC and AVP groups showed higher loadings than the LT group (ps < .05); Males showed no treatment effects across conditions (ps > .48) (Fig. 5A1, A2).

PC2 (biphasic pattern) demonstrated significant main effects of Treatment (F = 7.82, p < .001, η_p^2 = 0.30) and Isthreaten (F = 9.76, p = .002, η_p^2 = 0.24). The AVP group showed higher PC2 loadings compared to other groups (AVP vs PLC: p =.006; AVP vs LT: p = .025), whereas LT-PLC showed no difference (p = .53). Threatening stimuli elicited higher loadings than non-threatening ones (p < .001). A significant Treatment × Isthreaten interaction revealed greater responses to threatening versus non-threatening stimuli in both drug groups (ps < .01), but not in PLC (p = .45) (Fig. 5B).

PC3 (triphasic pattern) showed a significant main effect of Isthreaten (F = 8.12, p = .005, η_p^2 = 0.22), with threatening stimuli eliciting higher loadings than non-threatening ones.

Relationships Between Principal Components and Individual Difference Variables

We examined correlations between pupillary response components and individual differences in anxiety changes (Post-Pre State Anxiety scores) and judged time-to-collision (jTTC).

The most notable finding was a moderate negative correlation between PC2 (biphasic pattern) and anxiety change scores (r = -0.302, p = .001) (Fig 5D). Further analysis comparing high-anxiety (top 20%) versus low-anxiety (bottom 20%) groups revealed significantly lower PC2 loadings in the high-anxiety group (M = -0.025, SD = 0.035) compared to the low-anxiety group (M = 0.010, SD = 0.03) (t = 3.22, p = .003, Cohen's d = 1.09). This suggests that individuals with increased anxiety showed stronger pupil dilation during stimulus presentation but enhanced constriction after stimulus offset and provides a behavioral link of the PC2 to subjective anxiety.

For behavioral responses, PC3 (triphasic pattern) showed a significant positive correlation with jTTC (r = 0.263, p = .004), indicating that slower responders exhibited a distinctive pattern of weakened dilation followed by enhanced constriction-dilation cycles. PC1 showed a marginal negative trend with jTTC (r = -0.169, p = .069), while PC2's correlation with jTTC was non-significant (r = 0.147, p = .114) (Fig 5E).

Associations Between FPCA-derived Components and Phase-specific Pupillary Features

PC1 showed strong positive correlations with pupil dilation state (r = 0.615) and change rate (r = 0.650) during stimulus presentation, while negatively correlating with baseline pupil diameter (r = -0.177), suggesting greater dilation potential in participants with smaller baseline pupils.

PC2 demonstrated strong positive correlations with post-stimulus pupil dilation state (r = 0.668) and change rate (r = 0.603), while showing a moderate negative correlation with during-stimulus pupil state (r = -0.352), capturing the inhibition-to-activation transition.

PC3 exhibited strong negative correlation with during-stimulus change rate (r = -0.580) and a moderate positive correlation with post-stimulus change rate (r = 0.337), reflecting temporal

dynamic regulation (Fig 5F). See Supplementary Materials for feature calculation details.

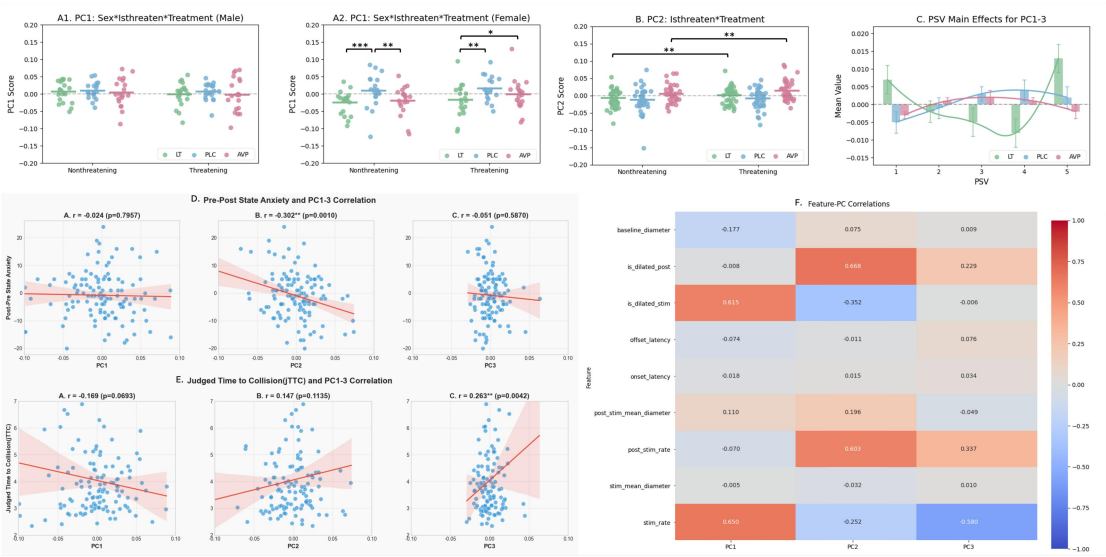

Fig 5. Relationships between pupillary principal components, experimental conditions, and individual differences. **(A)** Effects of sex, treatment, and threat conditions on PC1 loadings: **(A1)** No significant differences among treatments in males; **(A2)** In females, PLC group showed higher PC1 loadings than drug groups under non-threatening conditions, while PLC and AVP groups showed higher loadings than LT group under threatening conditions. **(B)** PC2 loadings across conditions: AVP group significantly higher than PLC and LT groups, and threatening stimuli higher than non-threatening stimuli; AVP and LT groups showed increased PC2 loadings under threat, while PLC group remained unchanged. **(C)** Principal component loadings across different speeds: PC1 sensitive to extreme speeds (V1,V5), PC2 increased with speed, PC3 more sensitive to medium speeds (V2-V4). **(D)** Negative correlation between PC2 and state anxiety change (Post-Pre) (r=-0.302, p=.001). **(E)** Positive correlation between PC3 and judged time-to-collision (jTTC) (r=0.263, p<.01). **(F)** Correlations between principal components and pupillary parameters: PC1 positively correlated with pupil dilation during stimulus presentation, PC2 positively correlated with post-stimulus pupillary changes but negatively with during-stimulus pupil state,

PC3 negatively correlated with during-stimulus change rate (r=-0.580) and positively with post-stimulus change rate (r=0.337). **p<.01.

Integration of Principal Component Patterns

PC1-3 captured distinct dynamic features of pupillary responses, with each component showing specific associations with experimental conditions and individual differences (Table 1).

Table 1 Summary of Functional Principal Component Features and Their Association Patterns

Principle Component	PC1	PC2	PC3
Variation Explanation	62.67%	17.56%	7.28%
Weight Time Function Features	Early steep rise followed by plateau	Initial inhibition, later strong activation	Early peak, mid-period trough, late recovery
Main Related Pupil Features	Stimulus-phase dilation (r=0.615) and dilation rate (r=0.65)	Post-stimulus dilation (r=0.668); Inverse relation to stimulus-phase dilation (r=-0.352)	Inverse stimulus-phase change rate (r=-0.580); Positive post-stimulus change rate (r=0.337)

Experimental Conditions	Female only: Nonthreatening: PLC>LT,PLC>AVP Threatening: PLC=AVP>LT Velocities: V1,V5>V2-V4 (No male differences)	AVP>LT, AVP>PLC Threat>Nonthreat V1,V2<V3-V5	Threat>Nonthreat V1,V5<V2-V3
Individual Differences	not significant	Low anxiety > High Anxiety	Early response < Late response
Possible Functional Significance	Sustained Vigilance and Attentional Resource Allocation	Threat-Specific Anxiety Response and Anticipatory Processing	Dynamic Transformation from Perception to Imagination

6.2 Pattern Identification and Classification

Multidimensional clustering analysis based on judged time-to-collision (jTTC) and pupillary functional principal components (PC1-PC3) identified eight distinct response patterns (Fig 6A). The stability of clustering was verified through bootstrap analysis (stability index: 0.753 ± 0.125) and five-fold cross-validation (0.651 ± 0.114; see S2 Fig). These patterns were primarily categorized by jTTC into early-response (E: 3.12 ± 0.57s) and late-response (L: 5.80 ± 1.98s) groups.

Among these patterns, E2 (n=1658) and L2 (n=1254) stood out with positive loadings across all principal components (PC1:+, PC2:+, PC3:+), reflecting similar patterns across components of vigilance, threat-specific anxiety response, and perception-to-imagination transformation but at different response times (early vs. late jTTC). Notably, E2 exhibited the highest PC1 loading (0.131), indicating the strongest vigilance-related dilation response.

Another notable pair was E1 (PC1:+, PC2:-, PC3: -) and L3 (PC1:-, PC2:+, PC3: +), which demonstrated opposing characteristics in both temporal and pupillary dynamics. E1 showed positive PC1 loading (0.041) with negative PC2/3, indicating enhanced initial vigilance but reduced threat-related processing, while L3 displayed most negative PC1 loading (-0.099) with positive PC2/3, showing suppressed early response but heightened threat sensitivity.

This pattern diversity reveals that individuals may employ different physiological-cognitive strategies when processing threat-related stimuli, even under similar behavioral response timing conditions. A detailed visualization of pattern distribution in PC1-PC2 space and comprehensive PC characteristics across all clusters can be found in Supplementary S3 Fig , which provides further evidence for the distinct separability among these response modes.

6.3 Steady State Distribution

Markov chain analysis identified E1, E3, and L1 as the dominant stable states across all treatments, with varying steady-state probabilities among groups. The placebo (PLC) group showed E1(24.4%), E3(18.1%), and L1(13.5%) as the most probable states, while distributions shifted in the LT group (E3:19.7%, E1:19.6%, L1:13.6%) and AVP group (E3:19.6%, E1:14.2%, L1:12.8%).

Treatment effects on steady-state distributions were significant ($\chi^2(14) = 333.17$, $p < .001$, Cramer' s $V = 0.107$). Residual analysis (Fig. 6B) revealed that Pattern E1 (PC1+, PC2-, PC3-) differentiated PLC from AVP groups (PLC: $z = 8.75$; AVP: $z = -9.85$), showing initial pupil dilation followed by constriction. In contrast, Pattern L3 (PC1-, PC2+, PC3+) showed higher steady states distribution in AVP and LT groups ($z = 4.96$ and 3.53) compared to PLC ($z = -8.32$), characterized by initial constriction and enhanced late activation. Pattern L2 (PC1+, PC2+, PC3+) distinguished AVP from LT, with elevated probability in AVP ($z = 3.57$) but reduced in LT ($z = -2.69$).

Isthreaten showed a significant main effect ($\chi^2(7) = 65.59$, $p < .001$, Cramer' s $V = 0.072$). Non-threatening conditions favored E1 patterns (20.5%, $z = 3.06$), while threatening stimuli shifted toward E2 patterns ($z = 4.21$). Particularly, Pattern E2 (PC1+, PC2+, PC3+), showing early pupil dilation with enhanced activation, emerged as a distinct stable state associated with threat processing. These characteristic patterns (E1, E2, L2, and L3) are illustrated through reconstructed pupillary responses in Fig. 6C, derived from PC scores and weights. Complete steady-state distribution results and heatmaps are available in Supplementary Materials, S4 Fig.

6.4 Dynamics Transition

Response patterns showed high self-transition probabilities (0.451-0.630) across all conditions, indicating stable response strategies. Self-transition probabilities varied by treatment: PLC group showed highest stability in E1(0.628) and L1(0.616); LT group exhibited comparable stability in E3(0.609) and E1(0.607); while AVP group was dominated by E3(0.630) and L3(0.583) patterns. All self-transitions were statistically significant (ps<.001).

Between-state transitions revealed treatment-specific characteristics. The most prominent transitions for each group were (see Fig. 6D for significant within-group transition paths): PLC group featured transitions toward E1 (E4→E1: 0.177; E3→E1: 0.175), LT group showed prominent E4→E1(0.166) and E2→E3(0.145) transitions, while AVP group was characterized by E1→E3(0.171) transitions (all *p*s<.01; full transition probabilities and 95% CIs from permutation tests are provided in S2 Table).

FDR-corrected group comparisons revealed distinct treatment effects on transition patterns. PLC group showed significantly increased probabilities in transitions targeting E1, including E1→E1(z = 2.39), E2→E1(z = 2.51), E3→E1(z = 4.65), and E4→E1(z = 2.49). In contrast, AVP group showed reduced transitions toward E1 (E1→E1: z = -4.30; E2→E1: z = -2.83; E4→E1: z = -3.40) but increased transitions involving L2 and L3 patterns (E4→L2: z = 2.92; L3→L3: z = 2.83; L1→L3: z = 2.54). LT group specifically showed reduced transitions toward L2 pattern (E2→L2: z = -2.32; E4→L2: z = -1.99) (all *p*s < .05; see S3 Table for 95% CIs and S5 Fig for detailed pairwise comparisons using permutation tests, n = 1000).

These results indicate that PLC enhances transitions toward E1(+,-,-), characterized by sustained vigilance but reduced threat-specific anxiety and perceptual-imaginative processing, whereas AVP promotes transitions toward patterns with opposite characteristics (E3/L3(-,+,+) and L3(+,+,+)) while reducing E1-directed transitions. LT does not facilitate any specific state transitions but selectively inhibits transitions toward L2(+,+,+), a pattern showing enhanced activation across all three components.

For threat effects, E3→E2 transitions were significantly modulated by Isthreaten (χ^2= 14.95, *p*-adj = .007), with increased probability under threatening conditions (z = 2.54) and decreased

probability under non-threatening conditions (z = -2.62).

6.5 Sequence Analysis

Analysis of 3×3 sequences revealed significant sequence differences across treatment conditions (χ^2= 247.63, p < .001). PLC group showed elevated probabilities in E1-related sequences, particularly self-transition (E1→E1→E1, z = 5.13, p < .001), transitional sequences including E1→E3→E1 (z = 2.96, p < .01), E3→E1→E1 (z = 2.42, p < .05), E1→E2→E1 (z = 2.66, p < .01) and E3→E1→E3 (z = 2.05, p < .05). Additionally, PLC exhibited higher probabilities in L1 self-transition (z = 3.05, p < .01), while showing reduced frequencies in sustained E3 (z = -2.87, p < .01) and L3 (z = -4.54, p < .001).

Conversely, AVP group demonstrated increased probabilities in sustained E3 (z = 3.69, p < .001) and L3 (z = 4.79, p < .001), while showing reduced probabilities in E1-related transitions, including both self-transition and and transition sequences (e.g., E1→E1→E3: z = -2.44, p < .05; E1→E3→E1: z = -2.54, p < .05; E4→E1→E1: z = -2.36, p < .05). LT group did not promote specific sequences but showed reduced probabilities in L1-related transition (e.g., L1→L1→L1, z = -2.23, p < .05; E3→E3→E1, z = -2.03, p < .05).

Markov sequence entropy analysis further supported these treatment-specific differences (ps < .001). LT group exhibited the highest sequence inconsistency (M = 8.02bit, 95% CI [7.96, 8.08]), significantly exceeding both AVP (M = 7.85bit, 95% CI [7.80, 7.91]; t = 130.70, p-adj < .001) and PLC groups (M = 7.76bit, 95% CI [7.70, 7.82]; t = 196.58, p-adj < .001). AVP group also showed higher entropy than PLC group (t = 71.06, p-adj < .001), indicating treatment-specific effects on behavioral state transitions and sequence inconsistency (Fig 6D).

While threat conditions did not yield significant sequence differences (χ^2 = 505.58, p = .54), entropy analysis revealed non-threatening stimuli induced significantly higher entropy than threatening stimuli (diff = 0.02bit, t = 20.13, p < .001), suggesting subtle but consistent threat effects on sequence inconsistency.

Fig 6. Pupillary Response Patterns and Transition Dynamics. (A) Principal component characteristics of early and late response patterns. Early response (E1-E4) and late response (L1-L4) patterns with their respective PC1-PC3 loadings. Red bars indicate negative contributions (opposite to the mean component trend), while blue bars indicate positive contributions (aligned with the mean component trend). Sample sizes are shown in parentheses. **(B)** Distribution of treatment groups across response clusters. Heatmap showing the relative frequency distribution of treatment groups (vertical axis) across eight response pattern clusters (horizontal axis). Color intensity represents relative frequency, ranging from deep red (high) to deep blue (low). Statistical significance is marked with asterisks (*p<.05, **p<.01, ***p<.001). **(C)** Pupillary dynamics

reconstruction of key response patterns. Reconstructed pupil diameter time courses based on PC1-3 temporal weight functions and pattern-specific PC scores. The vertical red dashed line represents stimulus offset, while the horizontal gray dashed line indicates baseline level (relative pupil diameter of zero). PLC group's typical pattern E1 shows sustained dilation during stimulus presentation followed by reduced dilation transitioning to constriction after stimulus offset. Drug groups (LT and AVP) show significantly higher representation in pattern L3, characterized by sustained constriction during stimulus presentation with reduced constriction after stimulus offset. AVP and LT groups show significantly higher representation in pattern L2, exhibiting progressively increasing dilation from stimulus onset to offset. Pattern E2, dominated by threat stimuli, shows pupillary characteristics similar to L2 but with earlier onset, indicating faster responses with high PC loadings in threatening situations. **(D)** Significant transition pathway networks across treatment groups. Circle nodes represent response patterns with self-transition probabilities shown inside. Connecting lines indicate between-state transitions, with line thickness representing transition probability magnitude. Red lines indicate significantly higher than random expectation, blue lines indicate significantly lower. **(E)** Sequence entropy distribution across treatment groups. Density curves showing the entropy distribution of pupillary response sequences across treatment groups, representing the complexity and predictability of response pattern transitions. The LT group (green) exhibits the highest entropy (highest variability), followed by AVP group (red), with PLC group (blue) showing the lowest entropy (highest stability). All between-group differences are significant (p-adj<.001).

Discussion

Our study examined the behavioral and pupillary dynamics of threat-modulated looming during stimulus approach and continued imagination of approach as well as modulation of these processes by two neuropeptides (vasopressin and angiotensin II) using a randomized placebo-controlled behavioral and eye-tracking design. The results demonstrate the dynamic processes underlying threat evaluation during different stages of the looming processes, their modulation by semantic context (threat) and function- and sex-dependent modulation by vasopressin and angiotensin signaling. Three key aspects emerge from our findings:

(1) The semantic (threat) modulation of the looming processes and in particular the temporal perception by threat-related content is modulated by velocity and sex, suggesting that the threat-induced temporal distortion adapts to dynamic characteristics of the threat and individual differences.

(2) Pupillometric analyses revealed a dynamic biphasic pupil response pattern characterized by sustained constriction during the visual approaching period (reaching maximum at stimulus disappearance), transitioning towards constriction release to progressive dilation prior to the expected (imagined) collision, which may reflect a dynamic interplay between vigilance and defensive responses.

(3) Examining the impact of the pharmacological modulation revealed that AVP did not modulate state anxiety on the subjective level but prolonged time-to-collision estimations and enhanced PC2 associated with reduced anxiety and enhanced patterns with prolonged vigilance (L2, L3) and transition into sustained high-arousal states. In contrast LT decreased subjective anxiety and promoted adaptive flexible responses such that LT enhanced sequence entropy and less anxiety-associated states.

Semantic modulation of the looming response: Temporal Judgment of Collision Under Threat

The modulatory effects of semantic context (threatening stimuli) and sex on the judged time to collision (jTTC) showed significant velocity-dependent characteristics. Under low to medium velocity conditions (V1-V4), jTTC estimates were shorter for threatening (vs. non-threatening) stimuli and for females (vs. males). These findings align with previous research using the looming paradigm showing that threatening stimuli result in underestimation of jTTC [7,10], and may reflect that females exhibit a more sensitive threat detection [49,50].

However, at the highest approach velocity (V5), both threat effects and sex differences disappeared simultaneously. The survival computation model suggests that approach velocity modulates threat assessment processes [51]. At slower velocities, the system can still decode the semantic content of the stimuli and allow threat-related modulation. When velocity exceeds a specific threshold the approaching stimulus may per se represent a threat and the system may switch into automated defense mode at the cost of decoding the content [52,53]. Neuroimaging studies have found that rapidly approaching threats enhance activity in defense-related regions including the amygdala, PAG and insula, while simultaneously reducing activity in prefrontal regulatory regions [54–57], suggesting that high-velocity approaching objects trigger defensive responses which override stimulus details and sex-differences. This likely reflects an evolutionarily adaptive mechanism prioritizing rapid defensive strategies over detailed processing in survival-critical situations [8].

Dynamic pupil response patterns: Pupillary Response of Threat Processing and Approach Velocity

Pupillary responses revealed two key characteristics of threat processing. During the visual stimulus approach phase, the pupils progressively constricted. Previous research shows that pupil constriction is dependent on decoding the content of stimuli [58–60] and may reflect the attentional focus on threatening stimuli [25]. During the subsequent imagination phase (after the stimulus disappearance) pupils showed progressive dilation. This pupillary change in the absence of external stimuli aligns with multiple studies [25,61,62] and may reflect the relationship between pupillary responses and emotional arousal. Pupil dilation reflects the internal mental representation but is also modulated by cognitive effort and anticipatory activation of defense systems [63]. This putative transition from visual processing of the looming stimulus towards an uncertainty-related defensive preparation corresponds with the attention-defense cascade model of threat processing proposed by Bradley [64].

Beyond these basic dynamics, approach velocity significantly modulated pupillary responses. Pupils exhibited a V-shaped response pattern to velocity, with threatening stimuli reaching maximum constriction at slower velocities (V2), while non-threatening stimuli required higher velocities (V4) to achieve maximum constriction. This underscores that threat-related content and velocity interact and suggest an preferential processing of threatening looming stimuli (see also previous findings on threat-enhanced perceptual processing, e.g. [32].

Based on FPCA analysis, we extracted three principal components (PC1-PC3) from trial-level pupillary responses, associated with distinct processes: PC1 reflects general arousal (associated with overall autonomic system activation, [65,66]); PC2 represents threat-specific

responses (consistent with threat sensitivity-related pupillary dynamics, [67–69]; PC3 embodies temporal processing capability (pupils as indicators of internal brain states modulating subjective time perception, [70,71]. This multidimensional separation may mirror coordinated action of multiple neural systems in threat processing [72,73]. Cluster analysis based on pupillary and behavioral characteristics identified eight response patterns, with threatening stimuli specifically enriched in the E2 pattern characterized by a high loading of all three components (PC1:+, PC2:+, PC3:+), demonstrating coordinated recruitment of high arousal, heightened vigilance, and enhanced temporal sensitivity during threat-related stimuli.

In addition, the pupillary dynamics showed sex-differences such that - at the overall response level - males showed larger pupillary responses in non-threatening contexts; temporally, females exhibited unique dynamic response patterns to threatening stimuli, particularly showing stronger threat-specific pupil dilation when collision was imminent. These sex differences reflect distinct processing characteristics in risk assessment: males demonstrated relatively stable cognitive processing patterns with higher exploratory responses in non-threatening contexts, while females showed more sensitive dynamic adaptation patterns with stronger vigilance responses and higher engagement of defensive processes to imminent threats [74–76].

Neuropeptide Modulation of the Looming Response

Determining effects of treatment revealed that AVP and LT influence threat information processing dynamics, yet via different subjective, behavioral and pupillary processes.

AVP induced no changes in state anxiety yet prolonged time-to-collision estimates which may reflect a temporal dilation. The findings may align with previous observations suggesting that

AVP enhances amygdalar processing of threat information [14,77] and attentional resource allocation towards salient stimuli [39,78] which in the context of the attention-gating theory may promote an extended time perception [79,80]. Moreover, other studies have demonstrated that AVP activates the sympathetic nervous system [81], increasing the sampling frequency of interoceptive information in the right anterior insula (AIC) and as such may result in time overestimation [82]. In contrast the LT group did not exhibit altered time-to-collision estimates, yet reported lower subjective anxiety levels as assessed by state anxiety assessments which may reflect an anxiolytic potential of AT1R blockade and aligns with previous studies reporting decreased neurofunctional fear expression [83], reduced amygdala activity in high-trait anxious individuals[16] and enhanced implicit fear regulation [84].

Pupillary data further revealed common and distinct effects of AVP and LT. At baseline, the AVP group showed significantly larger pupil diameter, which may reflect elevated autonomous arousal levels [85]. After baseline correction, both AVP and LT groups showed reduced pupil diameters compared to PLC during stimulus approach and early post-stimulus periods. Following stimulus disappearance and approaching collision, however, the treatments differentially modulated threat responses: While the PLC group exhibited a gradual weakening of threat-induced constriction—ultimately eliminating the initial threat/non-threat differentiation—both drug groups demonstrated a reversal to threat-evoked dilation (threat > non-threat). Critically, during this phase, the AVP group showed significantly larger threat-evoked dilation than PLC, while the LT group maintained smaller responses yet preserved threat sensitivity (threat > non-threat). In accordance the effects of AVP on baseline pupil diameters the larger responses to threat may reflect enhanced sympathetic activity and threat-related arousal,

vigilance or salience [86,87]. In combination with the decreased subjective anxiety the overall smaller pupil responses preserved threat/non-threat differentiation following LT which may reflect that AT1R blockades attenuated sympathetic reactivity without impairing threat detection [88,89].

The complex modulatory effects on the velocity-threat interaction further support this interpretation. While PLC showed velocity-dependent fluctuations in threat discrimination, distinct drug effects emerged: The AVP group showed larger responses to threatening versus non-threatening stimuli across all velocities (V1-V5), suggesting enhanced threat sensitivity or vigilance. In contrast, LT selectively enhanced threat detection at rapid velocities (V3-V5), possibly reflecting optimized amygdala-prefrontal filtering for high-relevance stimuli, balancing threat vigilance with attenuated anxiety [16,90,91].

HMM analysis allowed to further characterize the dynamic differences among the three groups. The PLC group showed a stable baseline pattern: primarily maintaining state E1(+,-,-) and characterized by transitions from other states to E1. Based on the behavioral characterization of the three pupillary components, this state may reflect enhanced general vigilance (PC1) but lower threat-specific anxiety (PC2) and temporal transition dynamics (PC3). The lowest state transition entropy supported this baseline vigilance state's stability.

The AVP group exhibited bistable distribution characteristics: L2(+,+,+) and L3(-,+,+). The L2 state shared similar pupillary characteristics with threat-associated E2(+,+,+) but with delayed response - consistent with the prolonged jTTC observed behaviorally, indicating its behavioral link with threat processing. While the L3 state may reflect a weakened early vigilance, it maintained threat processing and temporal transition dynamics. The transition matrix showed AVP inhibited transitions to E1 while promoting transitions to L2/L3, which may reflect AVPs role in

modulating temporal dynamics of threat-related processing [92].

The LT group demonstrated a differential modulatory pattern: (1) significantly higher occurrence only in L3(-,+,+) state, (2) inhibited transitions to E2 without promoting transitions to any specific states, (3) highest state transition entropy. The E2 state, characterized by sustained pupil dilation, reflects comprehensive activation of vigilance, threat-specific anxiety, and temporal expectancy, typically associated with excessive threat anticipation [93]. The suppression of E2 may further relate to the decreased subjective anxiety experienced following LT and suggest its therapeutic potential in contexts of heightened vigilance and threat anticipation, aligning with its proposed preventive effect of arousal-associated memory bias [94,95].

Notably, these treatment effects were sexually dimorphic. Females demonstrated enhanced pupillary responses compared to males under placebo, consistent with previously reported stronger sympathetic reactivity and vigilance biases [96,97]. Treatment-specific sex differences emerged with LT uniformly constricting female pupils, while AVP selectively suppressed non-threat responses in females, suggesting enhanced threat-specific resource allocation [98]. This sex-specific modulation reveals distinct mechanisms: LT may produce a general attenuation of arousal and anxiety, while AVP may specifically affect threat-related processing.

In conclusion, AVP and LT influence basal threat processing through distinct neural modulatory mechanisms, as revealed by both temporal dynamics and sex-specific effects. AVP promotes sustained threat monitoring through bistable high-arousal states (L2/L3) while sharpening female threat vigilance via non-threat suppression. In contrast, LT facilitates more flexible processing by promoting dynamic state transitions and reducing excessive activation (suppressing E2), with anxiety reduction in females. These mechanisms may indicate that AVP

may be applied for disorders with impaired threat detection (e.g., PTSD) and LT may by applied for conditions of pathological hyperarousal (e.g., generalized anxiety). This functional dissociation not only provides the direct evidence for sex-specific neuropeptide modulation of threat circuits, but also opens new avenues for developing personalized treatments for stress-related disorders.

Our study has several limitations. First, while we analyzed pupillary and behavioral responses, we did not examine their link to neural activation patterns. Future work could combine pupillometry with neuroimaging to directly map these relationships. Second, although chromatic differences existed between stimulus phases (colored vs. grayscale), our key findings—such as threat-specific pupillary dilation and pharmacological modulation—were consistent across matched conditions, suggesting cognitive-emotional rather than light reflex. Nevertheless, strictly controlled visual properties in future designs would strengthen validity. Finally, our principal component interpretations, while aligned with theoretical frameworks (e.g., arousal modulation, threat detection networks), remain inferential. Empirical validation of these components' neural substrates is needed.

Data Availability: All group-level data (including judged Time-To-Collision, anxiety ratings, and blood pressure measurements) will be made publicly available upon acceptance in the Open Science Framework (OSF) repository (DOI will be provided upon publication). Processed pupil data and additional materials can be obtained from the corresponding author upon reasonable request.

Funding: This research was supported by the STI 2030-Major Projects, Grant No.

2022ZD0208500, Ministry of Science and Technology of China.

Reference

1. Gao N, Wang H, Xu X, Yang Z, Zhang T. Angiotensin II induces cognitive decline and anxiety-like behavior via disturbing pattern of theta-gamma oscillations. Brain Res Bull. 2021;174: 84–91. doi:10.1016/j.brainresbull.2021.06.002

2. Liu X, Jiao G, Zhou F, Kendrick KM, Yao D, Gong Q, et al. A neural signature for the subjective experience of threat anticipation under uncertainty. Nat Commun. 2024;15: 1544. doi:10.1038/s41467-024-45433-6

3. Taschereau-Dumouchel V, Kawato M, Lau H. Multivoxel pattern analysis reveals dissociations between subjective fear and its physiological correlates. Mol Psychiatry. 2020;25: 2342–2354. doi:10.1038/s41380-019-0520-3

4. Thieu MK, Ayzenberg V, Lourenco SF, Kragel PA. Visual looming is a primitive for human emotion. iScience. 2024;27: 109886. doi:10.1016/j.isci.2024.109886

5. Zhou F, Geng Y, Xin F, Li J, Feng P, Liu C, et al. Human extinction learning is accelerated by an angiotensin antagonist via ventromedial prefrontal cortex and its connections with basolateral amygdala. Biol Psychiatry. 2019;86: 910–920. doi:10.1016/j.biopsych.2019.07.007

6. Card G, Dickinson M. Performance trade-offs in the flight initiation of drosophila. J Exp Biol. 2008;211: 341–353. doi:10.1242/jeb.012682

7. Schiff W. Perception of impending collision: A study of visually directed avoidant behavior. Psychological Monographs: General and Applied. 1965;79: 1–26. doi:10.1037/h0093887

8. Yilmaz M, Meister M. Rapid innate defensive responses of mice to looming visual stimuli. Current Biology. 2013;23: 2011–2015. doi:10.1016/j.cub.2013.08.015

9. Cooper WE, Samia DSM, Blumstein DT. Chapter five - FEAR, spontaneity, and artifact in economic escape theory: A review and prospectus. In: Naguib M, Brockmann HJ, Mitani JC, Simmons LW, Barrett L, Healy S, et al., editors. Advances in the Study of Behavior. Academic Press; 2015. pp. 147–179. doi:10.1016/bs.asb.2015.02.002

10. Vagnoni E, Lourenco SF, Longo MR. Threat modulates perception of looming visual stimuli. Current Biology. 2012;22: R826–R827. doi:10.1016/j.cub.2012.07.053

11. Cole S, Balcetis E, Dunning D. Affective signals of threat increase perceived proximity. Psychol Sci. 2013;24: 34–40. doi:10.1177/0956797612446953

12. Brendel E, Hecht H, DeLucia PR, Gamer M. Emotional effects on time-to-contact judgments: Arousal, threat, and fear of spiders modulate the effect of pictorial content. Exp Brain Res. 2014;232: 2337–2347. doi:10.1007/s00221-014-3930-0

13. Huber D, Veinante P, Stoop R. Vasopressin and oxytocin excite distinct neuronal populations in the central amygdala. Science. 2005;308: 245–248. doi:10.1126/science.1105636

14. Meyer-Lindenberg A, Domes G, Kirsch P, Heinrichs M. Oxytocin and vasopressin in the human brain: Social neuropeptides for translational medicine. Nat Rev Neurosci. 2011;12:

524–538. doi:10.1038/nrn3044

15. Thompson RR, George K, Walton JC, Orr SP, Benson J. Sex-specific influences of vasopressin on human social communication. Proc Natl Acad Sci U S A. 2006;103: 7889–7894. doi:10.1073/pnas.0600406103

16. Reinecke A, Browning M, Klein Breteler J, Kappelmann N, Ressler KJ, Harmer CJ, et al. Angiotensin regulation of amygdala response to threat in high-trait-anxiety individuals. Biol Psychiatry Cogn Neurosci Neuroimaging. 2018;3: 826–835. doi:10.1016/j.bpsc.2018.05.007

17. Zhang R, Zhao W, Qi Z, Xu T, Zhou F, Becker B. Angiotensin II regulates the neural expression of subjective fear in humans: A precision pharmaco-neuroimaging approach. Biol Psychiatry Cogn Neurosci Neuroimaging. 2023;8: 262–270. doi:10.1016/j.bpsc.2022.09.008

18. Xu T, Zhou X, Jiao G, Zeng Y, Zhao W, Li J, et al. Angiotensin antagonist inhibits preferential negative memory encoding via decreasing hippocampus activation and its coupling with the amygdala. Biological Psychiatry: Cognitive Neuroscience and Neuroimaging. 2022;7: 970–978. doi:10.1016/j.bpsc.2022.05.007

19. Szczepanska-Sadowska E. Role of neuropeptides in central control of cardiovascular responses to stress. J Physiol Pharmacol. 2008;59 Suppl 8: 61–89.

20. Höhle S, Culman J, Boser M, Qadri F, Unger T. Effect of angiotensin AT2 and muscarinic receptor blockade on osmotically induced vasopressin release. Eur J Pharmacol. 1996;300: 119–123. doi:10.1016/0014-2999(95)00855-1

21. von Bohlen und Halbach O, Albrecht D. The CNS renin-angiotensin system. Cell Tissue Res. 2006;326: 599–616. doi:10.1007/s00441-006-0190-8

22. Guo F, Zou J, Wang Y, Fang B, Zhou H, Wang D, et al. Human subcortical pathways automatically detect collision trajectory without attention and awareness. PLOS Biology. 2024;22: e3002375. doi:10.1371/journal.pbio.3002375

23. Armstrong T, Bilsky SA, Zhao M, Olatunji BO. Dwelling on potential threat cues: An eye movement marker for combat-related ptsd. Depression and Anxiety. 2013;30: 497–502. doi:10.1002/da.22115

24. Chen L, Yuan X, Xu Q, Wang Y, Jiang Y. Subliminal impending collision increases perceived object size and enhances pupillary light reflex. Front Psychol. 2016;7. doi:10.3389/fpsyg.2016.01897

25. Mathôt S, Van der Stigchel S. New light on the mind's eye: The pupillary light response as active vision. Curr Dir Psychol Sci. 2015;24: 374–378. doi:10.1177/0963721415593725

26. Joshi S, Li Y, Kalwani RM, Gold JI. Relationships between pupil diameter and neuronal activity in the locus coeruleus, colliculi, and cingulate cortex. Neuron. 2016;89: 221–234. doi:10.1016/j.neuron.2015.11.028

27. Hernández-Pérez OR, Hernández VS, Nava-Kopp AT, Barrio RA, Seifi M, Swinny JD, et al. A Synaptically Connected Hypothalamic Magnocellular Vasopressin-Locus Coeruleus Neuronal Circuit and Its Plasticity in Response to Emotional and Physiological Stress. Front Neurosci. 2019;13. doi:10.3389/fnins.2019.00196

28. Gong W, Lü J, Wang F, Wang B, Wang M, Huang H. Effects of angiotensin type 2 receptor on secretion of the locus coeruleus in stress-induced hypertension rats. Brain Research Bulletin. 2015;111: 62–68. doi:10.1016/j.brainresbull.2014.12.011

29. LeDoux JE, Brown R. A higher-order theory of emotional consciousness. Proceedings of the National Academy of Sciences. 2017;114: E2016–E2025. doi:10.1073/pnas.1619316114

30. Mobbs D, Hagan CC, Dalgleish T, Silston B, Prévost C. The ecology of human fear: Survival optimization and the nervous system. Front Neurosci. 2015;9. doi:10.3389/fnins.2015.00055

31. Mineka S, Öhman A. Phobias and preparedness: The selective, automatic, and encapsulated nature of fear. Biological Psychiatry. 2002;52: 927–937. doi:10.1016/S0006-3223(02)01669-4

32. Phelps EA. Emotion and cognition: Insights from studies of the human amygdala. Annual Review of Psychology. 2006;57: 27–53. doi:10.1146/annurev.psych.56.091103.070234

33. Watson D, Clark LA, Tellegen A. Development and validation of brief measures of positive and negative affect: The PANAS scales. Journal of Personality and Social Psychology. 1988;54: 1063–1070. doi:10.1037/0022-3514.54.6.1063

34. Spielberger CD. State-trait anxiety inventory for adults. 2012. doi:10.1037/t06496-000

35. Heimberg RG, Horner KJ, Juster HR, Safren SA, Brown EJ, Schneier FR, et al. Psychometric properties of the liebowitz social anxiety scale. Psychological Medicine.

1999;29: 199–212. doi:10.1017/S0033291798007879

36. Vetter RS. Calling all arachnophobic entomologists: A request for information. American Entomologist. 2012;58: 199–201. doi:10.1093/ae/58.4.199

37. Garver-Apgar CE, Gangestad SW, Thornhill R. Hormonal correlates of women's mid-cycle preference for the scent of symmetry. Evolution and Human Behavior. 2008;29: 223–232. doi:10.1016/j.evolhumbehav.2007.12.007

38. Gao Z, Ma X, Zhou X, Xin F, Gao S, Kou J, et al. Oxytocin reduces the attractiveness of silver-tongued men for women during mid-cycle. Front Neurosci. 2022;16. doi:10.3389/fnins.2022.760695

39. Zhuang Q, Zheng X, Becker B, Lei W, Xu X, Kendrick KM. Intranasal vasopressin like oxytocin increases social attention by influencing top-down control, but additionally enhances bottom-up control. Psychoneuroendocrinology. 2021;133: 105412. doi:10.1016/j.psyneuen.2021.105412

40. Kou J, Zhang Y, Zhou F, Sindermann C, Montag C, Becker B, et al. A randomized trial shows dose-frequency and genotype may determine the therapeutic efficacy of intranasal oxytocin. Psychological Medicine. 2022;52: 1959–1968. doi:10.1017/S0033291720003803

41. Quintana DS, Smerud KT, Andreassen OA, Djupesland PG. Evidence for intranasal oxytocin delivery to the brain: Recent advances and future perspectives. Therapeutic Delivery. 2018 [cited 5 Apr 2025]. doi:10.4155/tde-2018-0002

42. Berger A, Kiefer M. Comparison of different response time outlier exclusion methods: A simulation study. Front Psychol. 2021;12. doi:10.3389/fpsyg.2021.675558

43. Ratcliff R. Methods for dealing with reaction time outliers. Psychological Bulletin. 1993;114: 510–532. doi:10.1037/0033-2909.114.3.510

44. Hayes TR, Petrov AA. Mapping and correcting the influence of gaze position on pupil size measurements. Behav Res. 2016;48: 510–527. doi:10.3758/s13428-015-0588-x

45. Kret ME, Sjak-Shie EE. Preprocessing pupil size data: Guidelines and code. Behav Res. 2019;51: 1336–1342. doi:10.3758/s13428-018-1075-y

46. Laeng B, Sulutvedt U. The eye pupil adjusts to imaginary light. Psychological Science. 2013 [cited 3 Apr 2025]. doi:10.1177/0956797613503556

47. de Gee JW, Colizoli O, Kloosterman NA, Knapen T, Nieuwenhuis S, Donner TH. Dynamic modulation of decision biases by brainstem arousal systems. Stephan KE, editor. eLife. 2017;6: e23232. doi:10.7554/eLife.23232

48. Renner LF, Włodarczak M. When a dog is a cat and how it changes your pupil size: Pupil dilation in response to information mismatch. Interspeech 2017. ISCA; 2017. pp. 674–678. doi:10.21437/Interspeech.2017-353

49. Zambetti PR, Schuessler BP, Kim JJ. Sex differences in foraging rats to naturalistic aerial predator stimuli. iScience. 2019;16: 442–452. doi:10.1016/j.isci.2019.06.011

50. Glicksohn J, Hadad Y. Sex differences in time production revisited. Journal of Individual

Differences. 2012;33: 35–42. doi:10.1027/1614-0001/a000059

51. Mobbs D, Headley DB, Ding W, Dayan P. Space, time, and fear: Survival computations along defensive circuits. Trends Cogn Sci. 2020;24: 228–241. doi:10.1016/j.tics.2019.12.016

52. Mobbs D, Marchant JL, Hassabis D, Seymour B, Tan G, Gray M, et al. From threat to fear: The neural organization of defensive fear systems in humans. J Neurosci. 2009;29: 12236–12243. doi:10.1523/JNEUROSCI.2378-09.2009

53. Mobbs D, Hagan CC, Dalgleish T, Silston B, Prévost C. The ecology of human fear: Survival optimization and the nervous system. Front Neurosci. 2015;9. doi:10.3389/fnins.2015.00055

54. Mobbs D, Yu R, Rowe JB, Eich H, FeldmanHall O, Dalgleish T. Neural activity associated with monitoring the oscillating threat value of a tarantula. Proceedings of the National Academy of Sciences. 2010;107: 20582–20586. doi:10.1073/pnas.1009076107

55. Liu D, Li S, Ren L, Liu X, Li X, Wang Z. Different coding characteristics between flight and freezing in dorsal periaqueductal gray of mice during exposure to innate threats. Animal Model Exp Med. 2022;5: 491–501. doi:10.1002/ame2.12276

56. Zhou Z, Liu X, Chen S, Zhang Z, Liu Y, Montardy Q, et al. A VTA GABAergic neural circuit mediates visually evoked innate defensive responses. Neuron. 2019;103: 473-488.e6. doi:10.1016/j.neuron.2019.05.027

57. LeDoux JE, DS. Using neuroscience to help understand fear and anxiety: A two-system framework. AJP. 2016;173: 1083–1093. doi:10.1176/appi.ajp.2016.16030353

58. Barbur JL, Harlow AJ, Sahraie A. Pupillary responses to stimulus structure, colour and movement. Ophthalmic and Physiological Optics. 1992;12: 137–141. doi:10.1111/j.1475-1313.1992.tb00276.x

59. Naber M, Hilger M, Einhäuser W. Animal detection and identification in natural scenes: Image statistics and emotional valence. J Vis. 2012;12: 25. doi:10.1167/12.1.25

60. Naber M, Nakayama K. Pupil responses to high-level image content. J Vis. 2013;13: 7. doi:10.1167/13.6.7

61. Laeng B, Sulutvedt U. The eye pupil adjusts to imaginary light. Psychol Sci. 2014;25: 188–197. doi:10.1177/0956797613503556

62. Henderson RR, Bradley MM, Lang PJ. Emotional imagery and pupil diameter. Psychophysiology. 2018;55: e13050. doi:10.1111/psyp.13050

63. Leuchs L, Schneider M, Czisch M, Spoormaker VI. Neural correlates of pupil dilation during human fear learning. NeuroImage. 2017;147: 186–197. doi:10.1016/j.neuroimage.2016.11.072

64. Bradley MM, Miccoli L, Escrig MA, Lang PJ. The pupil as a measure of emotional arousal and autonomic activation. Psychophysiology. 2008;45: 602–607. doi:10.1111/j.1469-8986.2008.00654.x

65. Samuels ER, Szabadi E. Functional neuroanatomy of the noradrenergic locus coeruleus: Its roles in the regulation of arousal and autonomic function part I: principles of functional organisation. Curr Neuropharmacol. 2008;6: 235–253. doi:10.2174/157015908785777229

66. Reimer J, McGinley MJ, Liu Y, Rodenkirch C, Wang Q, McCormick DA, et al. Pupil fluctuations track rapid changes in adrenergic and cholinergic activity in cortex. Nat Commun. 2016;7: 13289. doi:10.1038/ncomms13289

67. Wirkner J, Weymar M, Löw A, Hamm AO. Effects of pre-encoding stress on brain correlates associated with the long-term memory for emotional scenes. PLOS ONE. 2013;8: e68212. doi:10.1371/journal.pone.0068212

68. Löw A, Bradley MM, Lang PJ. Perceptual processing of natural scenes at rapid rates: Effects of complexity, content, and emotional arousal. Cogn Affect Behav Neurosci. 2013;13: 860–868. doi:10.3758/s13415-013-0179-1

69. Bradley MM, Sapigao RG, Lang PJ. Sympathetic ANS modulation of pupil diameter in emotional scene perception: Effects of hedonic content, brightness, and contrast. Psychophysiology. 2017;54: 1419–1435. doi:10.1111/psyp.12890

70. Terhune DB, Sullivan JG, Simola JM. Time dilates after spontaneous blinking. Current Biology. 2016;26: R459–R460. doi:10.1016/j.cub.2016.04.010

71. Suzuki TW, Kunimatsu J, Tanaka M. Correlation between pupil size and subjective passage of time in non-human primates. J Neurosci. 2016;36: 11331–11337. doi:10.1523/JNEUROSCI.2533-16.2016

72. LeDoux JE, Pine DS. Using neuroscience to help understand fear and anxiety: A two-system framework. AJP. 2016;173: 1083–1093. doi:10.1176/appi.ajp.2016.16030353

73. Pessoa L, Adolphs R. Emotion processing and the amygdala: From a “low road” to “many roads” of evaluating biological significance. Nat Rev Neurosci. 2010;11: 773–783. doi:10.1038/nrn2920

74. Voulo ME, Parsons RG. Response-specific sex difference in the retention of fear extinction. Learn Mem. 2017;24: 245–251. doi:10.1101/lm.045641.117

75. Wester SR, Vogel DL, Pressly PK, Heesacker M. Sex differences in emotion: A critical review of the literature and implications for counseling psychology. The Counseling Psychologist. 2002;30: 630–652. doi:10.1177/00100002030004008

76. Cross CP, Campbell A. Women’s aggression. Aggression and Violent Behavior. 2011;16: 390–398. doi:10.1016/j.avb.2011.02.012

77. Croiset G, Nijsen MJMA, Kamphuis PJGH. Role of corticotropin-releasing factor, vasopressin and the autonomic nervous system in learning and memory. European Journal of Pharmacology. 2000;405: 225–234. doi:10.1016/S0014-2999(00)00556-2

78. Thompson R, Gupta S, Miller K, Mills S, Orr S. The effects of vasopressin on human facial responses related to social communication. Psychoneuroendocrinology. 2004;29: 35–48. doi:10.1016/s0306-4530(02)00133-6

79. Pariyadath V, Eagleman D. The effect of predictability on subjective duration. PLOS ONE.

2007;2: e1264. doi:10.1371/journal.pone.0001264

80. Tse PU, Intriligator J, Rivest J, Cavanagh P. Attention and the subjective expansion of time. Perception & Psychophysics. 2004;66: 1171–1189. doi:10.3758/BF03196844

81. Hasser EM, Cunningham JT, Sullivan MJ, Curtis KS, Blaine EH, Hay M. Area postrema and sympathetic nervous system effects of vasopressin and angiotensin II. Clinical and Experimental Pharmacology and Physiology. 2000;27: 432–436. doi:10.1046/j.1440-1681.2000.03261.x

82. Di Lernia D, Serino S, Pezzulo G, Pedroli E, Cipresso P, Riva G. Feel the time. Time perception as a function of interoceptive processing. Front Hum Neurosci. 2018;12. doi:10.3389/fnhum.2018.00074

83. Zhang R, Zhao W, Qi Z, Xu T, Zhou F, Becker B. Angiotensin II regulates the neural expression of subjective fear in humans: A precision pharmaco-neuroimaging approach. Biol Psychiatry Cogn Neurosci Neuroimaging. 2023;8: 262–270. doi:10.1016/j.bpsc.2022.09.008

84. Zhou F, Geng Y, Xin F, Li J, Feng P, Liu C, et al. Human extinction learning is accelerated by an angiotensin antagonist via ventromedial prefrontal cortex and its connections with basolateral amygdala. Biol Psychiatry. 2019;86: 910–920. doi:10.1016/j.biopsych.2019.07.007

85. McDougal DH, Gamlin PD. Autonomic control of the eye. Compr Physiol. 2015;5: 439–473. doi:10.1002/cphy.c140014

86. Nasimi A, Kafami M. Vasopressin and sympathetic system mediate the cardiovascular effects of the angiotensin II in the bed nucleus of the stria terminalis in rat. Neuroscience Research. 2016;108: 34–39. doi:10.1016/j.neures.2016.01.003

87. Spiga F, Walker JJ, Terry JR, Lightman SL. HPA axis-rhythms. Compr Physiol. 2014;4: 1273–1298. doi:10.1002/cphy.c140003

88. Ma X, Sigmund CD, Hingtgen SD, Tian X, Davisson RL, Abboud FM, et al. Ganglionic action of angiotensin contributes to sympathetic activity in renin-angiotensinogen transgenic mice. Hypertension. 2004;43: 312–316. doi:10.1161/01.HYP.0000111835.16662.43

89. Saxena PR. Interaction between the renin-angiotensin-aldosterone and sympathetic nervous systems. J Cardiovasc Pharmacol. 1992;19 Suppl 6: S80-88. doi:10.1097/00005344-199219006-00013

90. Gold AL, Morey RA, McCarthy G. Amygdala-prefrontal cortex functional connectivity during threat-induced anxiety and goal distraction. Biol Psychiatry. 2015;77: 394–403. doi:10.1016/j.biopsych.2014.03.030

91. Ranjbar H, Aghaei I, Moosazadeh M, Shabani M. Angiotensin II type 1 receptor blocker losartan attenuates locomotor, anxiety-like behavior, and passive avoidance learning deficits in a sub-chronic stress model. Iran J Basic Med Sci. 2018;21: 856–862. doi:10.22038/IJBMS.2018.27113.6632

92. Heinrichs M, von Dawans B, Domes G. Oxytocin, vasopressin, and human social behavior. Frontiers in Neuroendocrinology. 2009;30: 548–557. doi:10.1016/j.yfrne.2009.05.005

93. Grupe DW, Nitschke JB. Uncertainty and anticipation in anxiety: An integrated neurobiological and psychological perspective. Nat Rev Neurosci. 2013;14: 488–501. doi:10.1038/nrn3524

94. Shkreli L, Woud ML, Ramsbottom R, Rupietta AE, Waldhauser GT, Kumsta R, et al. Angiotensin involvement in trauma processing-exploring candidate neurocognitive mechanisms of preventing post-traumatic stress symptoms. Neuropsychopharmacology. 2020;45: 507–514. doi:10.1038/s41386-019-0553-y

95. Xu T, Zhou X, Jiao G, Zeng Y, Zhao W, Li J, et al. Angiotensin antagonist inhibits preferential negative memory encoding via decreasing hippocampus activation and its coupling with the amygdala. Biol Psychiatry Cogn Neurosci Neuroimaging. 2022;7: 970–978. doi:10.1016/j.bpsc.2022.05.007

96. Bianchin M, Angrilli A. Gender differences in emotional responses: A psychophysiological study. Physiology & Behavior. 2012;105: 925–932. doi:10.1016/j.physbeh.2011.10.031

97. Etgen AM, Karkanias GB. Estrogen regulation of noradrenergic signaling in the hypothalamus. Psychoneuroendocrinology. 1994;19: 603–610. doi:10.1016/0306-4530(94)90044-2

98. Thompson RR, George K, Walton JC, Orr SP, Benson J. Sex-specific influences of vasopressin on human social communication. Proceedings of the National Academy of Sciences. 2006;103: 7889–7894. doi:10.1073/pnas.0600406103

S1 Fig. Participant screening and randomization flow chart.

S2 Fig. Classification and Validation of Temporal-Dynamic Patterns in Pupillary Response. Top Left: Distribution of log-transformed response time (Log-jTTC), showing two natural groupings of early response (blue) and late response (orange). Top Right: Clustering validation metrics (Silhouette Score and Normalized CH Score) across different numbers of clusters (2-5), showing increasing CH Score with higher cluster numbers. Bottom Left: Bootstrap stability index distribution (red dashed line: mean of 0.753; green dashed lines: ±1 standard deviation). Bottom Right: Five-fold cross-validation stability scores (red dashed line: mean stability of approximately 0.7).

S3 Fig. Principal Component Analysis of Identified Response Patterns. Left: Distribution of data points in PC1-PC2 space with color-coded clusters representing different response patterns. Right: Heatmap displaying PC1, PC2, and PC3 values for each of the eight identified patterns (E1-E4: early response patterns; L1-L4: late response patterns), showing principal component characteristics for each cluster.

S4 Fig. Standardized Residuals of Factors across Response Pattern Clusters. Chi-square and residual analysis examining differential distributions across early (E1-E4) and late (L1-L4) response patterns for: Treatment (top left: LT, PLC, AVP); Sex (top right: Male, Female); IsThreaten (bottom left: Nonthreatening, Threatening); and Physical Stimulus Velocity (PSV) (bottom right: V1-V5). Values represent standardized residuals, with $|z| > 1.96$ indicating significantly higher or lower frequencies than expected by chance. Cramer's V values indicate effect size for each factor.

S5 Fig. Treatment group differences in transition probabilities. Each matrix shows pairwise comparisons between treatment groups (left: PLC-LT; middle: PLC-AVP; right: AVP-LT). The

rows represent current states and columns represent next states. Cell values indicate the difference in transition probabilities between groups (e.g., in PLC-LT matrix, positive/red values indicate higher probabilities in PLC compared to LT group). Black boxes highlight significant transitions (p-adj < .05). Color intensity corresponds to the magnitude of probability differences, with red indicating positive differences and blue indicating negative differences. For example, in the PLC-LT comparison, transitions toward L3 state show significantly lower probabilities in PLC compared to LT group, as indicated by blue cells with black borders. Transition probabilities were analyzed using permutation tests (n=1000) with FDR correction.

S1 Table. Demographics and questionnaire scores between treatment groups.

S2 Table. Within-treatment estimated transition probabilities and 95% confidence intervals from the bootstrap permutation test (1000 iterations).

S3 Table. Between-treatment differences in transition probabilities and 95% confidence intervals from the bootstrap permutation test (1000 iterations).